AIAA 81-0364R

Load Distribution on Multielement Deformed Airfoils with Gap Effects

J. M. Abernathy* and J. E. Burkhalter†
Auburn University, Auburn, Alabama

The aerodynamic loading for deformed wings with elevons in subsonic flow is considered. The solution procedure falls into the potential flow category with appropriate restrictions. Lifting surface Kernel function formulation is used in which the local pressure loading for both wing and elevon is determined simultaneously and written as a summation equation. The solution procedure allows closed-form results to be obtained for the elevon hinge moments. Cases under study include gaps between wing and elevon in addition to arbitrary wing-elevon deformations. Fuselage effects and leading-edge suction are also used to apply results to a general configuration. Results for all cases compare very well with experimental data. Experimental data taken in a low-speed wind tunnel are presented for a cropped delta wing and rectangular elevon in which the wing-elevon gap was the primary test variable.

Nomenclature

$\mathcal{R}$ = aspect ratio
b = wing span
B_{nm} = wing loading coefficients
B_{pq} = elevon loading coefficients
c = local wing chord
$\bar{c}$ = mean aerodynamic chord of the configuration (excluding gap length), reference length
c_{R_E} = root chord of elevon
c_{T_E} = tip chord of elevon
cc_l = section lift force/q_∞
c^2c_m = section pitching moment/q_∞
C_H = hinge moment coefficient
C_L = lift coefficient
C_M = pitching moment coefficient about wing root chord leading edge
C_p = pressure coefficient $(p-p_\infty)/q_\infty$
I = integral of the chordwise term of the pressure loading function, see Eq. (12)
L = lift force on the wing
M_∞ = freestream Mach number
q_∞ = freestream dynamic pressure
S = wing-elevon planform area (excluding gap area), reference area
w = nondimensional perturbation velocity parallel to z axis
x,y,z = Cartesian coordinates
α = angle of attack
β = Mach flow parameter, $\sqrt{1-M_\infty^2}$
δ = elevon angle relative to wing (trailing edge down is positive)
ϵ = gap width between wing trailing edge and elevon leading edge
Λ = wing leading-edge sweep angle
θ = nondimensional spanwise variable
ξ,η = nondimensional variables, see Eq. (2)

Subscripts

E = elevon
H = hinge characteristics
HL = hinge line
LE = leading edge
nm = points or constants associated with the wing
pq = points or constants associated with the elevon
T = total
TE = trailing edge
VLE = leading-edge vortex
W = wing
0 = denotes wing coordinate variables
∞ = freestream conditions

Introduction

RESEARCH in theoretical aerodynamics in the past has been dominated by attempts to obtain better, more exact solutions to the basic equations which govern the flow over a single lifting surface. In recent years, major efforts have been put forth to model the flow over multielement airfoils and to predict the resulting loads and moments. Most of the research efforts concerning these multielement lifting surfaces have been two-dimensional analyses, as typified by the early work of Glauert[1,2] in 1924 and 1927 and more recently by the work of Halsey.[3] However, the case of a wing/air gap/ control surface combination has generally been neglected as pointed out by Ashley,[4] who also expressed the need for such an analysis.

Extension of analyses to include three-dimensional effects or finite wings has generally employed vortex lattice formulations or some form of constant pressure paneling such as that of Woodward[5] or Lan.[6] The Lan approach has received considerable attention of late since the leading-edge suction terms and Kutta condition at the trailing edge are properly accounted for in the analysis. DeJarnette[7] extended the "strip" approach of Lan to provide for a "continuous" loading in the spanwise direction. Aside from the Lan-DeJarnette formulation, general vortex lattice approaches suffer from traditional shortcomings such as large computer storage and long run times, even on today's high-speed computers. Formulation of the problem using the Kernel function approach in its usual form, typified by Cunningham,[8] has generally been neglected but offers the potential for increased accuracy, lower computer run times, and less storage than does the vortex lattice approach. An example of the potential for the Kernel function approach for a two-dimensional airfoil with a gap is presented by Nissim and Lottati[9] where comparisons are made with the vortex lattice method and the method of Lan.[6]

Both the vortex lattice and Kernel function approaches have enjoyed certain success but certainly the vortex lattice has been more extensively used. There are certain problems which, although amenable to vortex lattice solutions, are

Presented in part as Paper 81-0364 at the AIAA 19th Aerospace Sciences Meeting, St. Louis, Mo., Jan. 12-15, 1981; submitted July 22, 1981; revision received Dec. 23, 1981.

*Research Assistant, Aerospace Engineering. Member AIAA.
†Associate Professor, Aerospace Engineering. Member AIAA.

easily handled by Kernel function techniques, namely that of wing irregularities such as twist, camber, and arbitrary deformations. Certainly camber and twist have been addressed in previous efforts, but analyses of moderate "arbitrary" deformation of a lifting surface have not been found in the literature.

Wing-elevon configurations generally have been sealed gap cases. However, White and Landahl[10,11] have developed a procedure for determining the load distribution when a gap exists which requires the method of matched asymptotic expansions. This theory has many restrictions, including limitation to the two-dimensional case.

The present work is concerned with the wing-elevon problem for configurations with moderate wing deformations such as camber, twist, and general deformations due to high wing loading while still retaining nonseparated flow restrictions. Lifting surface theory is employed, with the solution following the procedure established by Purvis[12] and Burkhalter and Purvis.[13] The loading function over the multiple lifting surface is defined, and the Kernel function is then integrated over the surface. For this work, the gap distances are considered to be small enough that vortex rollup is assumed negligible.

Comparison is made with experimental data on several general configurations. For the gap case, data were obtained from low-speed wind-tunnel tests with gap distance as the primary test variable. Data for several elevon deflection angles and hinge line locations are shown for each configuration at numerous angles of attack. Experimental data are lacking for arbitrary wing deformations at subsonic speeds, but comparisons are made with wings which have moderate camber and twist.

Theoretical Analysis

Basic Equations of Lifting Surface Theory

The appropriate equations and solution procedure for the Kernel function which is employed in this analysis are well known[14,15] and the solution procedure is developed in detail in Ref. 12.

Using the Prandtl-Glauert transformation to include compressibility effects, the downwash at an arbitrary point (x,y) on a lifting surface is

$$w(x,y,0)=\frac{1}{8\pi}\int\int_S \frac{\Delta C_p(\eta,\xi)}{(y-y_0)^2} \times\left[1+\frac{(x-x_0)}{\sqrt{(x-x_0)^2+\beta^2(y-y_0)^2}}\right]dx_0dy_0 \tag{1}$$

where ξ and η are dimensionless chordwise and spanwise variables, respectively, defined as

$$\xi=\frac{x-x_{LE}(y)}{c(y)}, \qquad \eta=\frac{y}{b/2} \tag{2}$$

The functional form of the pressure loading coefficient is assumed as

$$\Delta C_p(\xi,\eta)=\sum_{n=0}^{N}\frac{1}{c(\eta)}\sum_{m=0}^{M}B_{nm}\sin(2m+1)\theta\sqrt{\frac{1-\xi}{\xi}}\,\xi^n \tag{3}$$

where $\eta=\cos\theta$, and N and M represent an arbitrary number of chordwise and spanwise control points, respectively. It is readily seen that this form produces the required leading-edge square root singularity, satisfies the Kutta condition at the trailing edge, and has slender wing behavior at the wing tips. A discussion of the logic behind this assumed form of the pressure loading is presented in Ref. 12.

Over a sufficiently small subpanel of the wing planform (Fig. 1), ΔC_p is essentially constant and may be taken outside the integral of Eq. (1) and the resulting expression may be evaluated in closed form.[12]

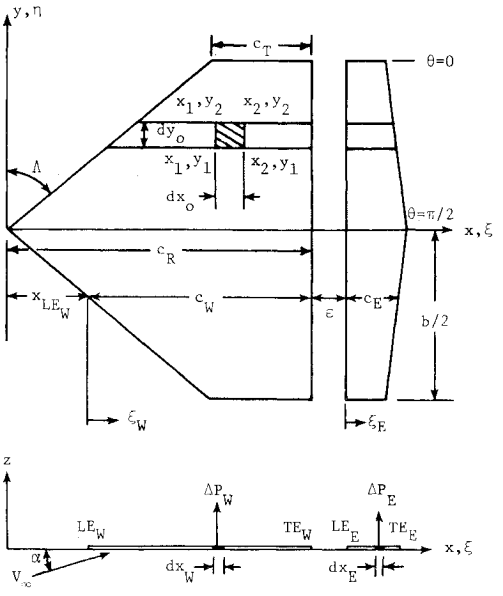

Fig. 1 Wing geometry and aerodynamic forces.

The boundary condition imposed is the requirement of no flow through the wing. As illustrated in Refs. 12 and 13, the total downwash at any control point due to the entire wing is found by summing the effect of each subpanel of the lifting surface and therefore the boundary condition becomes

$$\sum_S\sum\Delta w(x_i,y_j)+\sin\alpha(x_i,y_j)=0 \tag{4}$$

where (x_i,y_j) are the control points and are located according to a cosine distribution.[7] Thus a set of linear equations for the $N\times M$ unknown loading coefficients B_{nm}, defined by combining Eqs. (3) and (4), may now be solved simultaneously.

Loading Function for Wing/Gap/Elevon Configuration

When a control surface (elevon) is added to the wing, or when a gap is introduced between the wing and elevon, the loading distribution is, of course, changed. In the present work, it is assumed that the elevon span is equal to the wing span and the elevon hinge line is perpendicular to the wing centerline. With these restrictions, the solution procedure for the basic wing is parallel except for the loading function.

First, for the sealed-gap case with a deflected elevon, a two-function formulation using Eq. (3) to describe the pressure distribution is used. The nondimensional chordwise variable ξ of Eq. (3) is redefined and considered separately for the wing and elevon as

$$\xi_W=\frac{x-x_{LE_W}(y)}{c_W(y)+c_E(y)}, \qquad \xi_E=\frac{x-x_{LE_E}(y)}{c_E(y)} \tag{5}$$

This geometry is also shown in Fig. 1. With these definitions, it is easily verified that the leading-edge singularity is satisfied on both the wing and elevon and that the Kutta condition is met at the elevon trailing edge. These singularities agree with usual assumed loading functions with control surfaces as pointed out by Landahl.[11] At the wing trailing edge, the Kutta condition is not satisfied nor is the usual logarithmic singularity obtained, but rather a finite value is found. This loading is used in lieu of the logarithmic form in order to obtain a closed-form solution to the sectional lift integral. Error due to this assumption is considered to be on the same order as the assumption of an infinite loading, while the advantages of a closed-form solution are considerable.

When a gap exists between the wing and elevon, the loading function over the wing and elevon is defined in order to create the effect of two wings. The leading-edge singularity and

Kutta condition must be satisfied on each surface. Equation (3) produces this distribution by redefining the chordwise variables illustrated in Fig. 1 as

$$\xi_W = \frac{x - x_{LE_W}(y)}{c_W(y)}, \qquad \xi_E = \frac{x - x_{LE_E}(y)}{c_E(y)} \tag{6}$$

for the wing and elevon, respectively.

After the load distribution has been defined, the resulting set of linear equations contains unknown coefficients for both the wing and elevon. The summation is performed over the entire surface of the wing and elevon; thus, for the control points on the elevon, the boundary condition becomes

$$\sum_S \sum \Delta w(x_i, y_j) + \sin[\alpha(x_i, y_j) + \delta(x_i, y_j)] = 0 \tag{7}$$

It should be noted that the loadings for the wing and elevon are solved simultaneously; therefore, iteration of the interference between the surfaces is eliminated. The pressure at any point on the wing or elevon is given by Eq. (3), with the appropriate definition of ξ_W and ξ_E and the appropriate value of the B_{nm} (wing or elevon).

Total Aerodynamic Forces and Moments

From the wing-elevon configuration shown in Fig. 1, the total lift is given by integration of the pressure differential over the wing and elevon. Using the definition for the pressure coefficient, the lift produced by the wing and elevon is

$$L = q_\infty \int_{-b/2}^{b/2} \left\{ \int_{x_{LE_W}}^{x_{TE_W}} \Delta C_{p_W} \mathrm{d}x_W + \int_{x_{LE_E}}^{x_{TE_E}} \Delta C_{p_E} \mathrm{d}x_E \right\} \mathrm{d}y \tag{8}$$

and the sectional lift coefficient may be defined as

$$cc_l(\eta) = \int_0^{\xi_{TE_W}} \Delta C_{p_W}(\xi_W, \eta) c_{W_T} \mathrm{d}\xi_W + \int_0^1 \Delta C_{p_E}(\xi_E, \eta) c_E \mathrm{d}\xi_E \tag{9}$$

where

$$c_{W_T} = \begin{cases} c_W & \text{gap case} \\ c_W + c_E & \text{gap-sealed case} \end{cases} \tag{10}$$

Using Eq. (3) for the pressure distribution, the integration of Eq. (9) may be performed as in Ref. 13 to give

$$cc_l(\eta) = \sum_{n=0}^{N_W} \sum_{m=0}^{M} I_n B_{nm} \sin(2m+1)\theta + \sum_{p=0}^{N_E} \sum_{q=0}^{M} I_p B_{pq} \sin(2q+1)\theta \tag{11}$$

where B_{nm} represents the pressure loading coefficients corresponding to the wing loading and B_{pq} the coefficients of the elevon loading. Also, in Eq. (11), I_n and I_p represent the integration of the chordwise pressure terms[13] for the wing and elevon, respectively, as

$$I_n = \int_{LE_W}^{TE_W} \xi_W^n \sqrt{\frac{1-\xi_W}{\xi_W}} \mathrm{d}\xi_W, \quad I_p = \int_{LE_E}^{TE_E} \xi_E^p \sqrt{\frac{1-\xi_E}{\xi_E}} \mathrm{d}\xi_E \tag{12}$$

Similar manipulations lead to determination of the section pitching moment coefficient as

$$\begin{aligned} c^2 c_m(\eta) = {} & x_{LE_W} \sum_{n=0}^{N_W} \sum_{m=0}^{M} I_n B_{nm} \sin(2m+1)\theta \\ & + c_{W_T} \sum_{n=0}^{N_W} \sum_{m=0}^{M} I_{n+1} B_{nm} \sin(2m+1)\theta \\ & + x_{LE_E} \sum_{p=0}^{N_E} \sum_{q=0}^{M} I_p B_{pq} \sin(2q+1)\theta \\ & + c_E \sum_{p=0}^{N_E} \sum_{q=0}^{M} I_{p+1} B_{pq} \sin(2q+1)\theta \end{aligned} \tag{13}$$

where the first two terms are seen to be the moment due to the wing, and the last two are the moment due to the elevon.

For the wing alone, the integration of Eqs. (11) and (13) for the total lift and moment is performed analytically in closed form.[12] However, because of the discontinuity resulting from the addition of an elevon, these equations must be integrated numerically when a gap exists or the elevon is deflected.

Elevon Hinge Moments

Elevon hinge moments are determined in a manner similar to that of the wing pitching moments. For a straight elevon leading edge with the hinge line located at the leading edge, the total elevon hinge moment coefficient is

$$C_H = \frac{2}{S_E \bar{c}_E} \int_0^1 c^2 c_{m_H}(\eta) \mathrm{d}\eta \tag{14}$$

Considering both the wing and elevon contributions to the total pitching moment separately, it is noted that the sectional hinge moment coefficient, $c^2 c_{m_H}$, is given by the last term of Eq. (13). Substituting this term into Eq. (14), the integration may be evaluated in closed form[13] to obtain

$$\begin{aligned} C_H = {} & -\frac{2c_{R_E}}{S_E \bar{c}_E} \frac{\pi}{4} \sum_{p=0}^{N_E} B_{p1} I_{p+1} \\ & + \frac{c_{R_E} - c_{T_E}}{S_E \bar{c}_E} \sum_{p=0}^{N_E} \sum_{q=0}^{M} B_{pq} I_{p+1} G_q \end{aligned} \tag{15}$$

where

$$G_q = \int_0^{\pi/2} \sin 2\theta \, \sin(2q+1)\theta \mathrm{d}\theta \tag{16}$$

It is readily seen that the sectional lift of the elevon is the second integral in Eq. (9) and the solution is given by the last term of Eq. (11). The total lift may be obtained in closed form by integrating the last term in Eq. (11) in the spanwise direction resulting in

$$C_{L_E} = \frac{\pi}{2S_E} \sum_{p=0}^{N_E} B_{p0} I_p \tag{17}$$

where, in the loading coefficient B_{pq}, only the $q=0$ term appears.

Thus, using Eqs. (15) and (17), the elevon hinge moment about any hinge line location is obtained in closed form. The restrictions for the analysis are that the hinge line be perpendicular to the wing root chord and that the elevon span equals that of the wing.

Nonplanar Wings

To be precise, the nonplanar Kernel function should be used in the computation of downwash velocity components

for arbitrarily deformed wings. However, if the deformations are not severe such that nonseparated (potential) flow restrictions still apply, one may approximate the downwash with the planar downwash Eq. (1), provided that the appropriate induced velocity angles are included. With this approximation, the induced velocity at a control point due to a subpanel (see Fig. 1) of the wing or elevon may be written as

$$\Delta w(x_i,y_j) = \Delta w(x_i,y_j)_p \cos(\alpha_i - \alpha_c) \tag{18}$$

where $\Delta w(x_i,y_j)_p$ is the downwash computed for the planar wing. The surface slope angles, α_i and α_c, are measured relative to the x axis and defined by

$$\alpha_i = \tan^{-1}\left(\frac{\partial z}{\partial x}\right)\Big|_{x_i} \tag{19}$$

and

$$\alpha_c = \tan^{-1}\left(\frac{\partial z}{\partial x}\right)\Big|_{x_c} \tag{20}$$

where $\partial z/\partial x$ is the local slope of the deformed surface.

The function $z(x,y)$ defines the variations and amplitudes of camber, twist, and arbitrary wing deformation in the chordwise and spanwise direction.

Interference Effects

In the present analysis, fuselage perturbations and leading-edge suction are also included. An infinite line doublet is used to simulate fuselage interference effects on the wing and elevon. To calculate the lift and moment of a fuselage in the presence of a wing, an image wing inside the fuselage is employed. Both of these principles are well known and the theoretical development may be found in Ref. 16.

Leading-edge suction, which makes a significant contribution to the lift of highly swept wings at large angles of attack, has also been incorporated into the present theory. Purvis[17] has shown that, for an assumed pressure distribution in the form of Eq. (3) and for an elliptic spanwise lift distribution, a general, closed-form solution for the leading-edge suction is

$$C_{L_{VLE}} = \left(C_{L_p}\sin\alpha - \frac{C_{L_p}^2}{\pi R}\cos\alpha\right)\left(\frac{\cos\alpha}{\cos\Lambda}\right) \tag{21}$$

where C_{L_p} represents the potential flow lift coefficient.

The moment due to suction is given in Ref. 17 and for a constant leading-edge sweep angle, the result is

$$C_{M_{VLE}} = \frac{0.65151}{\bar{c}}\left[C_{L_p}\sin\alpha - \frac{C_{L_p}^2}{\pi R}\cos\alpha\right]\left(\frac{\tan\Lambda}{\cos\alpha}\right) \tag{22}$$

Since the current gap analysis assumes small gaps such that there is no significant wing vortex rollup effect on the elevon, interference effects will be confined to the fuselage doublet terms and the nonlinear lift terms will be confined to leading-edge suction.

Experimental Model and Tests

To verify gap effects and subsequent elevon loading, an experimental model (Fig. 2) was fabricated and tested in a low-speed wind tunnel.[18] The baseline configuration consisted of a thin, low-aspect-ratio, cropped delta wing with rectangular elevons. These surfaces were symmetrical about both the chord line and the fuselage centerline. The fuselage and wing tips were designed to allow for a 2 in. translation in the elevon mounting position, which could be used to vary the gap distance and/or the elevon hinge line location. The model was floor mounted to an external six-component pyramidal balance.

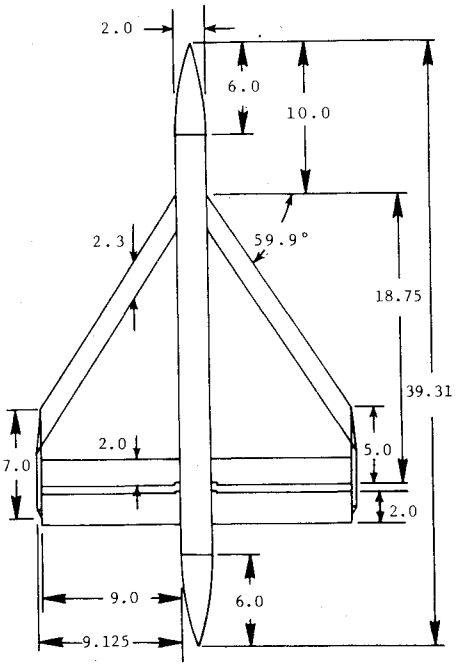

Fig. 2 Experimental model details.

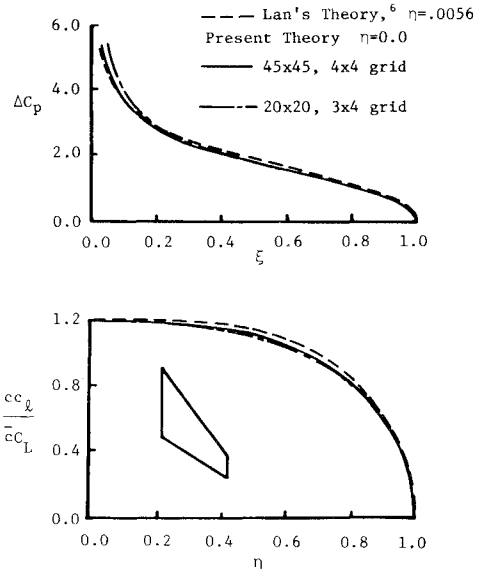

Fig. 3 Theoretical comparison of results for a swept and tapered wing.

The model was tested at a dynamic pressure of 8.9 cm of water corresponding to a speed of approximately 38.4 m/s and a Reynolds number of 2.49×10^6/m. Data were obtained for an angle-of-attack range from -19 to $+5$ deg in 2 deg increments. The negative range was used to minimize strut interference effects on the elevons. Several elevon deflection angles (0-20 deg), gap distances (0-75% c_E), and hinge line locations (0-50% c_E) were tested.

Results

Results for a wing of aspect ratio 2.828 (Warren 12 planform) are compared with the theory of Lan[6] in Fig. 3. In obtaining results using the present theory, the number of wing subpanels of constant loading was 45×45 (chordwise by spanwise) and the control point grid was 4×4. In practice, these numbers have proved to be sufficient for any configuration analyzed thus far. The total CPU time required was 45 s on an IBM 3031 compared to 1 min for the method of Lan on the Honeywell 635.[6] Storage requirements for the

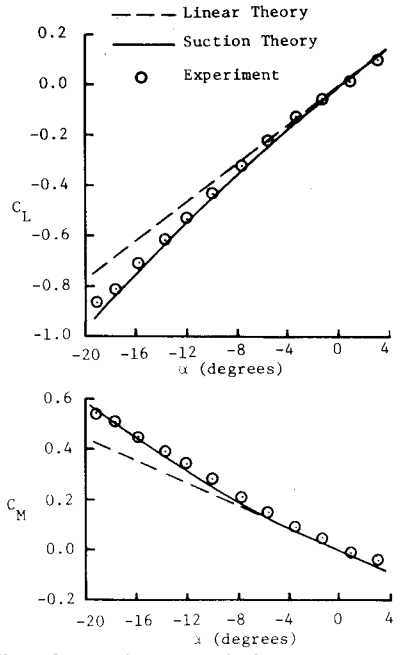

Fig. 4 Leading-edge suction on a highly swept cropped delta wing with fuselage.

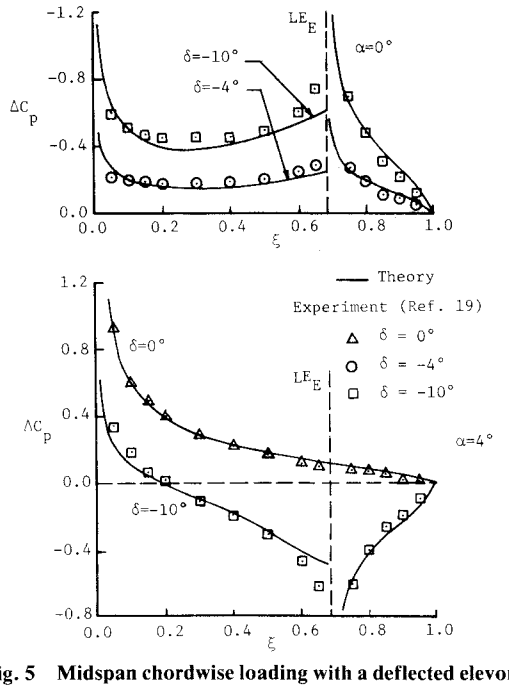

Fig. 5 Midspan chordwise loading with a deflected elevon.

present method are small on a large machine. The subpanel size was then reduced so that total CPU time was reduced to 15 s with little change in accuracy, as indicated on the figure.

A comparison of theory and experiment for the wing-fuselage portion of the model illustrated in Fig. 2 is presented in Fig. 4. Both linear theory and leading-edge suction are included. The importance of the nonlinearity introduced by leading-edge suction in the high angle-of-attack region is easily realized from this figure.

The theoretical pressure distribution for a finite wing with deflected elevon is compared with experimental data[19] in Fig. 5. From this figure it is seen that the assumed functional form for the chordwise pressure distribution for the sealed-gap case, although not the more correct logarithmatic form, is a good model of the actual flow. Integration in the spanwise direction to produce total lift and hinge moments also show good agreement with experimental data.[18]

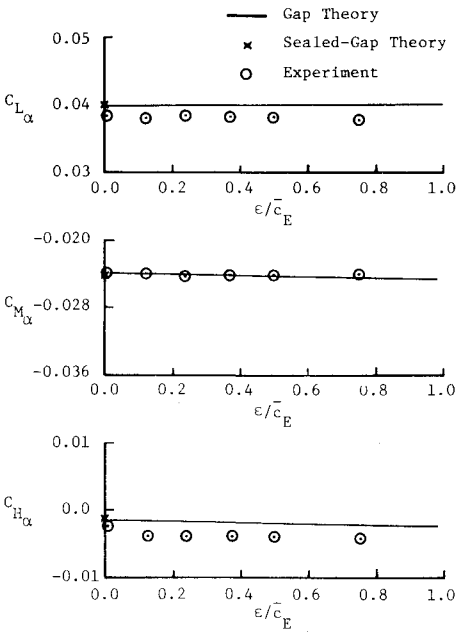

Fig. 6 Aerodynamic coefficient slope variation ($\partial/\partial\alpha$) with gap distance.

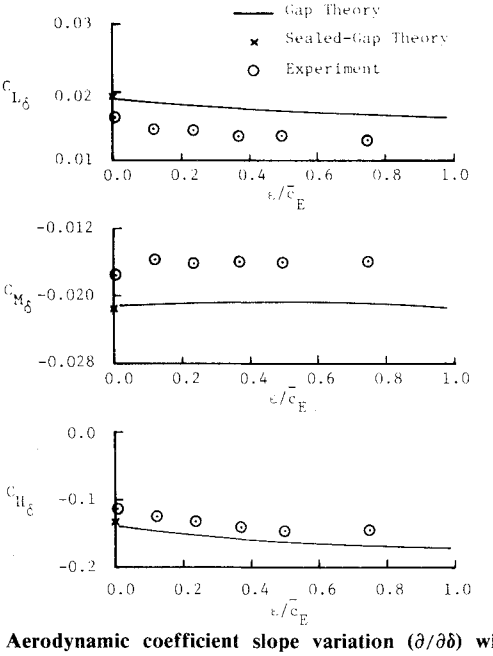

Fig. 7 Aerodynamic coefficient slope variation ($\partial/\partial\delta$) with gap distance.

The analysis developed for the general case of deformed wings, elevons, gap, and fuselage is used to predict the lift, pitching moment, and hinge moment slopes for the model tested in the low-speed tunnel and is shown as a function of gap distance in Figs. 6 and 7.

Certainly the most interesting trend with respect to the gap is that, for all cases, hinge moments increase slightly as gap distance increases. It is also noted from Figs. 6 and 7 that the coefficient slope variations with angle of attack are essentially independent of gap distance while variations with elevon deflection angle are significantly influenced by gap distance. Figure 8 illustrates the typical theoretical chordwise pressure distribution over the wing and elevon for this configuration. This figure confirms the predicted increase in the loading over the elevon and shows the slight loading change with respect to angle of attack. The form of the load distribution is in agreement with the two-dimensional results obtained by White and Landahl.[10]

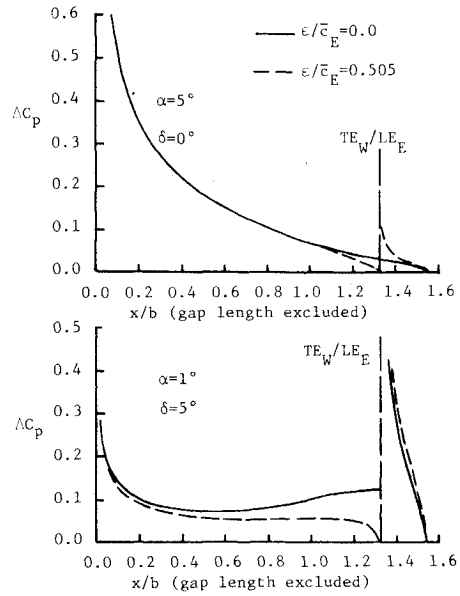

Fig. 8 Gap effects on chordwise load distribution.

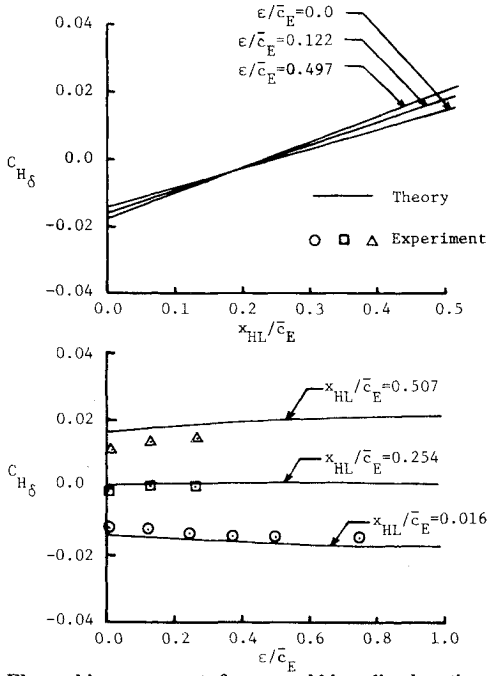

Fig. 9 Elevon hinge moments for several hinge line locations and gap distances.

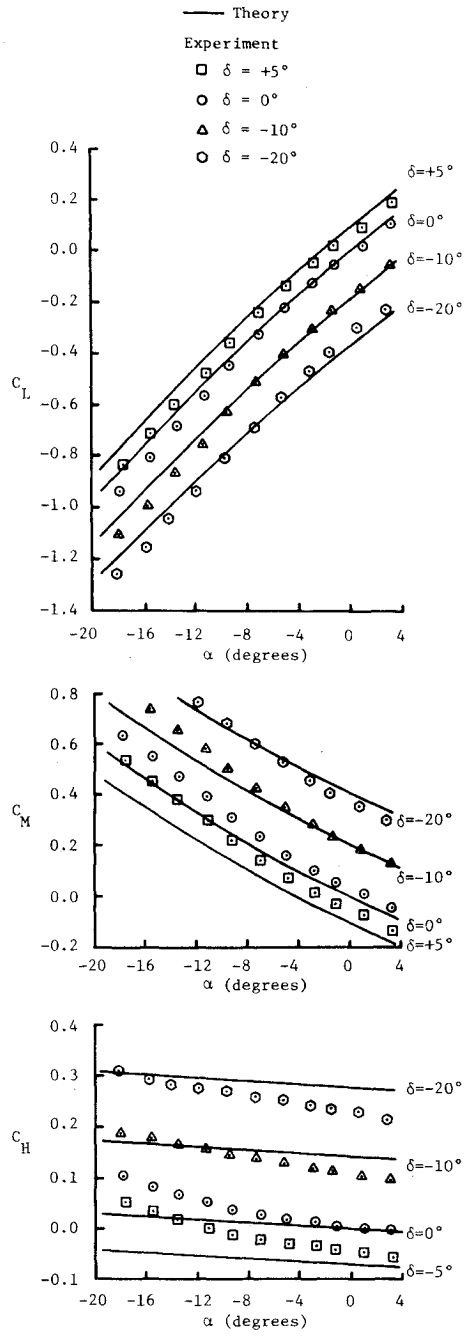

Fig. 10 Characteristics of the wing-fuselage-elevon model for $x_{HL}/\bar{c}_E = 0.016$ and $\epsilon/\bar{c}_E = 0.004$.

In Fig. 9, the hinge moments are presented for several hinge line locations on the elevon. It is seen here that there is a chordwise point, in this case between 15 and 20% of the elevon mean aerodynamic chord, where hinge moments are independent of gap distance. It is noted that this point does not coincide with $C_{H_\delta} = 0$, which gives the elevon aerodynamic center. This aspect could be significant in the design of variable geometry wings where gap distances are subject to change. Also, the minimum value of the hinge moment, which corresponds to minimum control forces, occurs for the sealed-gap case.

For large gaps, it was found experimentally (Figs. 10 and 11) that there is a considerable decrease in the total lift and moment for an elevon deflection of -20 deg. The decrease in the forces becomes larger with increased gap distance. However, elevon hinge moments do not reflect this trend, suggesting that it may be created by the presence of the gap rather than by flow separation over the elevon. Further experimental tests will be necessary to fully study this phenomenon.

Results for arbitrarily deformed airfoils are difficult to find in the literature; therefore, perhaps the best basis for comparison is two-dimensional thin-airfoil theory. Figure 12 illustrates theoretical results for two arbitrary mean lines. The present theory applied to two-dimensional configurations shows good agreement with thin-airfoil theory.

For a finite wing, Fig. 13 compares theoretical predictions with experimental data[20] at a Mach number of 0.6 for a wing that is both cambered (NACA $a = 1.0$ mean camber line) and twisted. It should be noted that the experimental model was tapered and the maximum camber varied with the spanwise coordinate. In the theoretical model, the mean camber line was recalculated only at 20% intervals along the span. Also, a linear spanwise distribution of twist was assumed, while there was a slight variation from this experimentally. Nonetheless, agreement of theory and experiment is very good.

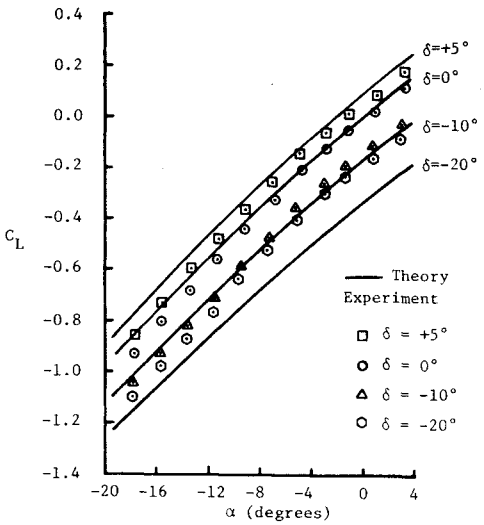

a)

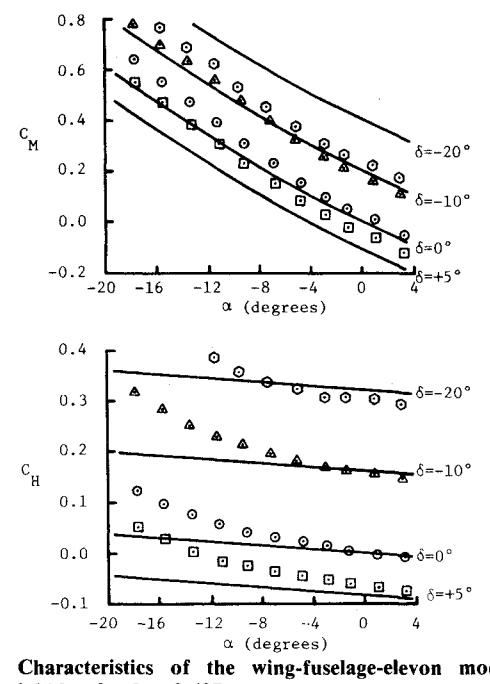

b)

Fig. 11 Characteristics of the wing-fuselage-elevon model for $x_{HL}/\bar{c}_E = 0.016$ and $\epsilon/\bar{c}_E = 0.497$.

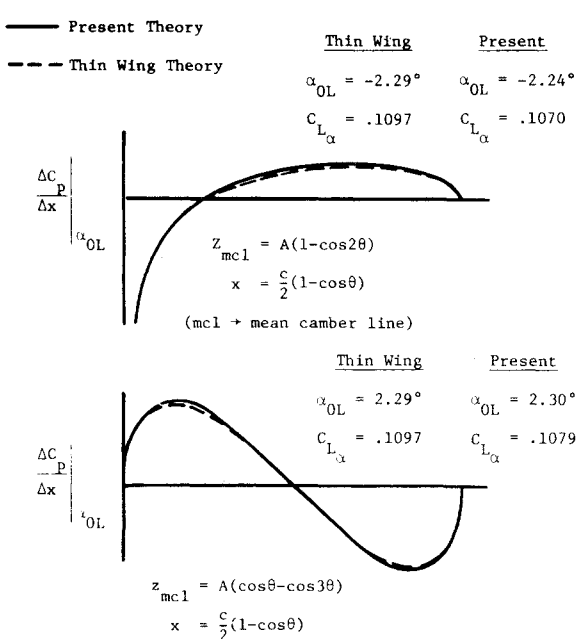

Fig. 12 Results for arbitrary mean lines.

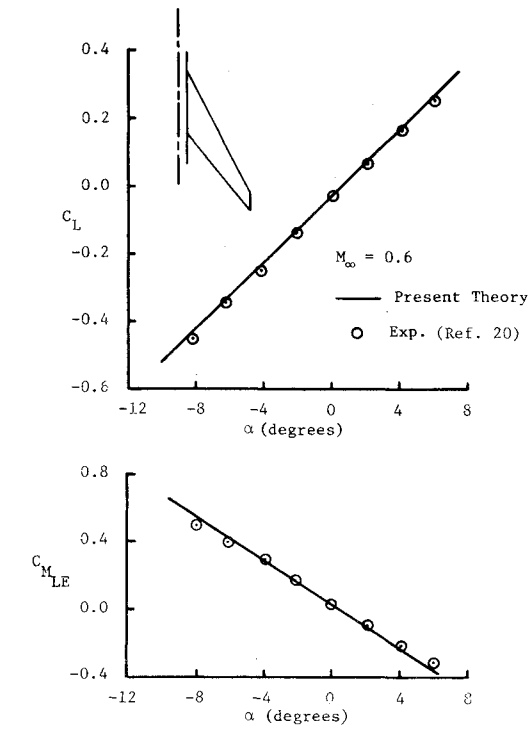

Fig. 13 Characteristics of a cambered and twisted finite wing with fuselage, $M_\infty = 0.6$.

Conclusions

A general theory that results in closed-form summation solutions for some of the aerodynamic coefficients has been developed by extending existing theories. Configurations ranging from a basic wing to varying combinations of wings, elevons, gap, and fuselage may be modeled as well as moderate wing and/or elevon deformations. From the preceding results, it is seen that the theory produces good results in the inviscid flow regime. Since compressibility effects are included, reasonable agreement with experiment up to large (subsonic) Mach numbers is obtained.

For the finite-gap case, the theory provides an excellent means for obtaining early design characteristics in a short time for small angles of attack and elevon deflections. However, it has been shown that for large elevon deflections there is a considerable decrease in total lift and moment coefficients when a large gap was present. This appears to be a viscous phenomenon and therefore cannot be modeled with potential flow techniques. Vortex rollup, which must be included for very large gaps, has also been neglected in the present theory. Results for cambered, twisted, and deformed wings may also be obtained easily with the present theory. Good results are obtained as long as the flow does not separate from the surface. No comparisons are made for arbitrary deformations on both the wing and elevon because of a lack of experimental data; however, the present theory still applies and calculations for these configurations appear encouraging.

Several advantages of the current method occur as a consequence of the assumption of a constant ΔC_p over a small subpanel of the wing. The wing can be divided into many subpanels, yet a relatively small matrix must be inverted to obtain the load distribution. This assumption allows ΔC_p to be taken outside the downwash integral and yields a closed-form solution to the equation. As a result, this method requires considerably smaller computational times and storage space than many methods, such as vortex lattice, which usually require a matrix equivalent in size to the number of wing subpanels.

The versatility illustrated by the theory suggests that further extensions can be made, for example, to partial span flaps

with lateral gaps and a hinge line that is swept with respect to the centerline. Also, the theory has already been extended to include wings with the curved leading and/or trailing edges.

Acknowledgments

Portions of this research were sponsored by the U.S. Army Research Office and the Army Missile Command under Contract DAAG29-78-G-0036. The experimental work was performed at Auburn University and sponsored by the Enginnering Experiment Station. The assistance of personnel at the Army Missile Command and the Army Research Office is greatly appreciated.

References

[1] Glauert, H., "A Theory of Thin Airfoils," British Aeronautical Research Committee, R&M 910, 1924.

[2] Glauert, H., "Theoretical Relationships for an Airfoil with Hinged Flap," British Aeronautical Research Committee, R&M 1095, 1927.

[3] Halsey, N.D., "Potential Flow Analysis of Multielement Airfoils Using Conformal Mapping," AIAA Paper 79-0271, Jan. 1979.

[4] Ashley, H., "Some Considerations Relative to the Prediction of Unsteady Air Loads on Interfering Surfaces," *Symposium on Unsteady Aerodynamics for Aeroelastic Analyses of Interfering Surfaces, Pt. I,* NATO AGARD-CP-80, April 1971.

[5] Woodward, F.A., "Analysis and Design of Wing-Body Combinations at Subsonic and Supersonic Speeds," *Journal of Aircraft,* Vol. 5, Nov.-Dec. 1968, pp. 528-534.

[6] Lan, C.E., "A Quasi-Vortex Lattice Method in Thin Wing Theory," *Journal of Aircraft,* Vol. 11, Sept. 1974, pp. 516-527.

[7] DeJarnette, F.R., "Arrangement of Vortex Lattices on Subsonic Wings," *Vortex-Lattice Utilization Workshop,* NASA SP-405, May 1976, pp. 301-323.

[8] Cunningham, A.M., "Unsteady Subsonic Collocation Method for Wings With and Without Control Surfaces," *Journal of Aircraft,* Vol. 9, June 1972, pp. 413-419.

[9] Nissim, E. and Lottati, I., "Oscillatory Subsonic Piecewise Continuous Kernel Function Method," *Journal of Aircraft,* Vol. 14, June 1977, pp. 515-516.

[10] White, R. and Landahl, M., "Effects of Gaps on the Loading Distribution of Planar Lifting Surfaces," *AIAA Journal,* Vol. 6, April 1968, pp. 626-631.

[11] Landahl, M., "Pressure-Loading Functions for Oscillating Wings with Control Surfaces," *AIAA Journal,* Vol. 6, Feb. 1968, pp. 345-348.

[12] Purvis, J.W., "Simplified Solution of the Compressible Subsonic Lifting Surface Problem," Master's Thesis, Aerospace Engineering Dept., Auburn University, Ala., Aug. 1975.

[13] Burkhalter, J.E. and Purvis, J.W., "An Aerodynamic Analysis of Deformed Wings in Subsonic and Supersonic Flow," Aerospace Engineering Dept., Auburn University, Ala., Final Report on U.S. Army Contract DAAG29-77-G-0069, Dec. 1977.

[14] Ashley, H. and Landahl, M., *Aerodynamics of Wings and Bodies,* Addison-Wesley, Reading, Mass., 1965.

[15] Ashley, H., Widnall, S., and Landahl, M., "New Directions in Lifting Surface Theory," *AIAA Journal,* Vol. 3, Jan. 1965, pp. 3-16.

[16] Pitts, W.C., Nielsen, J.H., and Kaattari, G.E., "Lift and Center of Pressure of Wing-Body-Tail Combinations at Subsonic, Transonic, and Supersonic Speeds," NACA Rept. 1307, 1957.

[17] Purvis, J.W., "Analytical Prediction of Vortex Lift," *Journal of Aircraft,* Vol. 18, April 1981, pp. 225-230.

[18] Abernathy, J.M., "An Analysis of Gap Effects on Wing-Elevon Aerodynamic Characteristics," Master's Thesis, Aerospace Engineering Dept., Auburn University, Ala., June 1980.

[19] Tinling, B.E. and Dickson, J.K., "Tests of a Model Horizontal Tail of Aspect Ratio 4.5 in the Ames 12-Foot Pressure Wind Tunnel, II: Elevon Hinge Line Normal to the Plane of Symmetry," NACA RM A9H11a, Oct. 1949.

[20] Jones, J.L. and Demele, F.A., "Aerodynamic Study of a Wing-Fuselage Combination Employing a Wing Swept Back 63°-Characteristics Throughout the Subsonic Speed Range with the Wing Cambered and Twisted for a Uniform Load at a Lift Coefficient of 0.25," NACA RM A9D25, Aug. 1949.